

# Exploring the Role of Water Molecules for Docking and Receptor Guided 3D-QSAR Analysis of Naphthyridine Derivatives as Spleen Tyrosine Kinase (Syk) Inhibitors

Maninder Kaur, Malkeet Singh Bahia, and Om Silakari\*

Molecular Modeling Lab (MML), Department of Pharmaceutical Sciences and Drug Research, Punjabi University, Patiala, Punjab, 147002, India

## S Supporting Information

**ABSTRACT:** In the present study, 3D-QSAR analysis was performed utilizing docking based alignment of [1,6]-naphthyridine derivatives as Syk enzyme inhibitors. The role of the water molecules was explored for the docking based alignment that revealed two conserved water molecules important for proper orientation and alignment of naphthyridine inhibitors in the active site of Syk enzyme. The QSAR model was selected having highest value of  $Q^2$  (0.624) and Pearson- $r$  (0.862). The selected model also displayed the highest values of  $R^2$  (0.978) and  $F$ -value (184.5) and the lowest SD (0.862). The contour plots developed on the basis of the best model helped to reveal the essential structural features of naphthyridines derivatives responsible for inhibition of Syk enzyme. The generated model and information revealed from it was utilized to design and predict new congeneric molecules that can be used as potential therapeutic agents.



## 1. INTRODUCTION

Spleen tyrosine kinase (Syk), a cytosolic nonreceptor tyrosine kinase, has recently been reported as a novel anti-inflammatory target. It is a member of Syk family kinase along with ZAP-70 and contains two Src homology 2 (SH2) domains and a kinase domain (371–631 amino acids).<sup>1</sup> Its secondary structure consists of 38% helical (11 helices; 111 residues) and 21%  $\beta$  sheet (14 strands; 63 residues). Ser 379, Val 385, Ala 400, Met 448, Glu 449, Ala 451, Glu 452, and Gly 454 form the substrate binding site.<sup>2</sup> It plays a critical role for Fc $\epsilon$ RI signaling in the mast cells and basophils that results in the release of a variety of inflammatory mediators,<sup>3</sup> suggesting that it can be explored as a potential therapeutic target in various inflammatory conditions such as allergic rhinitis, asthma, and anaphylaxis.<sup>4</sup> Furthermore, Syk is involved in the activation and signaling of the B-cell receptor<sup>5</sup> that uncovered an opportunity to suppress the formation of autoantibodies in a number of autoimmune disorders, e.g., rheumatoid arthritis and multiple sclerosis, etc.<sup>6</sup> Thus, the small molecule Syk inhibitors would serve as promising therapeutic agents for the treatment of various allergic and autoimmune disorders.

The charisma of Syk as therapeutic target can be described by a large number of patents and studies reported in the literature. In recent years, a noteworthy number of pharmaceutical companies and academic institutions have been involved in the development of small molecule Syk inhibitors. The diverse chemical classes of Syk inhibitors have been reported in the literature, e.g., 1,6-naphthyridines,<sup>7</sup> 1,2,4-triazolo[4,3c]pyrimidine,<sup>8</sup> 1,2,4-triazolo[1,5c]pyrimidine,<sup>8</sup> imidazo[1,2c]pyrimidine,<sup>9</sup> pyrimidine-5-carboxamide,<sup>10</sup> and 4-thiazolyl-2-phenylaminopyrimidines, etc.<sup>11</sup>

The general chemical structures of these classes are displayed in Figure 1. Rigel pharmaceuticals have developed Fostamatinib (R788), a prodrug of R406 which has completed phase-II of clinical trials.<sup>12,13</sup> R112, another compound developed by Rigel pharmaceuticals was also tested in phase-II clinical trials for symptomatic seasonal allergic rhinitis.<sup>14–17</sup> In December 2007, Pfizer started phase-I clinical trials for an inhaled formulation of R343 for the treatment of allergic asthma.<sup>18</sup>

In the present study, 3D-QSAR analysis of naphthyridine Syk inhibitors was performed. Naphthyridine molecules are ATP-competitive inhibitors of Syk. For this purpose, the docking based alignment of studied molecules was used. All the available crystal structures of protein Syk were employed to analyze the active site of enzyme and structural water molecules for the docking analysis. Afterward, the *Liaison* module of Schrodinger software was employed to cover the flexibility of enzyme's active site region. 3D-QSAR model generated this way was used to design and predict 27 new Syk inhibitors and subsequently the ADME properties of these inhibitors were calculated. These newly designed inhibitors can serve as good anti-inflammatory therapeutic agents in the future.

## 2. MATERIALS AND METHODS

**2.1. Data Set Selection.** For the present study, 49 congeneric naphthyridine Syk inhibitors were collected from the literature.<sup>7</sup> Out of these molecules, two were removed due to their unspecified stereochemistry and remaining 47 were

Received: May 13, 2012

Published: August 19, 2012



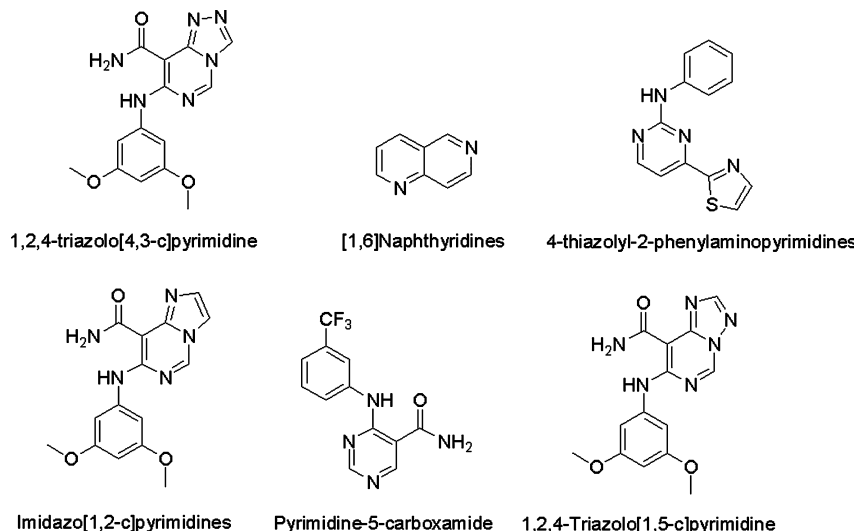


**Figure 1.** Various chemical classes of spleen tyrosine kinase (Syk) inhibitors.

considered for analysis. The reported biological activity of all collected molecules was determined experimentally using the same assay protocol.<sup>19</sup> All molecules exhibited a wide range of biological activity ( $IC_{50}$ ; 8–25 000 nM) and proper variation in structural features. The biological activity of molecules was converted into corresponding pIC<sub>50</sub> value (−log IC<sub>50</sub>).

**2.2. Molecular Modeling.** All studied molecules were sketched and cleaned using the “builder tools” option implemented in the “Maestro” molecular modeling program (version 9.2).<sup>20</sup> The molecules were then optimized with OPLS\_2005 force field using the “Ligprep” (version 2.5) module of Maestro at a pH value of 7.0 ± 0.1.<sup>21</sup>

**2.3. Docking Analysis.** For the docking analysis of all studied molecules, “Glide” (version 5.6) was used.<sup>22,23</sup> Glide consisted of two modes for docking processing named SP (Standard Precision) and XP (Extra Precision). For the present study, the XP mode of docking was used. Since no crystal structure of Syk with naphthyridine derivatives is available in the protein data bank (PDB), six crystal structures of Syk solved with different ligands,<sup>24–26</sup> i.e. 2-aminopyrimidine (1XBB), staurosporine (1XBC), 4-thiazolyl-2-phenylamino pyrimidine (3EMG), 2-aminopyrimidine (3FQS), 2-substituted-7-azaindole (3FQH), and 2-amino pyrimidine carboxamide (3FQE) were selected. All six complexes were optimized using the “protein preparation wizard” module implemented in the Maestro program and the optimization included completion of bond order, addition of hydrogen atoms, construction of missing side chains and loops. Finally, the complexes were minimized using an OPLS\_2005 force field to RMSD of 0.15 Å employing the “impref” option of the protein preparation wizard.

To analyze the active site and determine important water molecules, all protein complexes were aligned with their Cα backbone using the protein structure alignment option of Maestro.

**2.4. Protein and Ligand Complex Minimization.** A modeling program linear interaction approximation in implicit solvation (Liaison; version 5.7) of Schrodinger software was employed to minimize the complex of protein and ligand.<sup>27</sup> Liaison simulation combines a molecular mechanics calculation with experimental data to build a model scoring function used to correlate or to predict ligand–protein binding free energies. It is based on the assumption that binding energy can be

approximated by comparing energies of free and protein-bound ligand using the following empirical formula

$$\Delta G = \alpha(\langle U_{\text{bvdw}} \rangle - \langle U_{\text{fvdw}} \rangle) + \beta(\langle U_{\text{belec}} \rangle - \langle U_{\text{felec}} \rangle) + \gamma(\langle U_{\text{bcav}} \rangle - \langle U_{\text{fcav}} \rangle)$$

Where ⟨ ⟩ represents the ensemble average, b and f represents the bound and unbound form of the ligand, α, β, and γ are the coefficients,  $U_{\text{vdw}}$ ,  $U_{\text{elec}}$ , and  $U_{\text{cav}}$  are the van der Waals, electrostatic, and cavity energy terms in the surface generalized Born (SGB) continuum solvent model. The cavity energy term,  $U_{\text{cav}}$ , is proportional to the exposed surface area of the ligand. Thus, the difference  $\langle U_{\text{bcav}} \rangle - \langle U_{\text{fcav}} \rangle$  measures the surface area lost by the contact with receptor. In most applications, the coefficients α, β, and γ are determined empirically by fitting to the experimentally determined free energies of binding for training set ligands. In such applications, Liaison simulation task is used to calculate the values of  $U_{\text{vdw}}$ ,  $U_{\text{elec}}$ , and  $U_{\text{cav}}$  for the bound (complexed) and unbound (free) states of the training set ligands, and its analysis task is used to derive values for the α, β, and γ fitting coefficients. The fitted equation can then be used to predict the binding affinities of additional ligands. Liaison includes a constant term that is added to ΔG in the fitting process and is adjusted during the fit. This corresponds to an extension of the strict linear response model.

In the Liaison minimization, a portion of protein can be assigned as flexible, i.e. tiny (4/7), small (8/12), or medium (12/16). In the tiny option, the receptor region of 4 Å from the ligand is treated as flexible, from 4 to 7 Å as restrained, and beyond 7 Å as fixed. For the receptor ligand minimizations, we started with tiny, then progressed to small and medium. The complexes were minimized employing the Truncated Newton algorithm and OPLS\_2005 force field with 1000 steps for minimization.

**2.5. Selection of Training and Test Set Using the Canvas Program.** For the development of 3D-QSAR models, the data set was divided into training and test set on the basis of molecular properties employing the “Canvas” (version 1.4) module of Schrodinger software. In Canvas, the uniform distribution of structural variation was kept under consideration along with uniform distribution of activity.<sup>28,29</sup> Basically, Canvas performs clustering of the molecules on the basis of their molecular properties. For this, “binary fingerprints” were

computed for all molecules using MACCS structural keys and “*bit count*” was calculated. Then, “*hierarchical clustering*” was done for all molecules coupled with “*tanimoto similarity matrix*” calculation that cluster the molecules according to their properties considering one molecule as a centroid in each cluster. In the present study, total nine clusters were obtained and centroid molecule from each cluster was kept in training set (Table 1). The other molecules present in each cluster were kept in the training or test set according to proper distribution of the biological activity.

**Table 1. Results of Molecular Clustering Using the Canvas Program**

cluster no.	no. of molecules in cluster	total molecules
1	14	4, 7 <sup>a</sup> , 8, 10, 11, 13, 14, 15, 16, 17, 18, 23, 24, 26
2	1	25 <sup>a</sup>
3	5	1, 3 <sup>a</sup> , 6, 9, 12
4	1	31 <sup>a</sup>
5	1	21 <sup>a</sup>
6	12	36, 38, 32, 33, 34, 35, 27, 28, 19 <sup>a</sup> , 20, 22, 3
7	3	37, 39 <sup>a</sup> , 40
8	2	30 <sup>a</sup> , 29
9	1	2 <sup>a</sup>

<sup>a</sup>Centroid molecule of the corresponding cluster.

**2.6. 3D-QSAR.** Quantitative structure activity relationship (QSAR), in simplest terms, is a method for building computational or mathematical model that attempts to find a statistically significant correlation between structure and biological activity using a chemometric technique like partial least-squares (PLS) analysis, etc. For the development of 3D-QSAR models, PHASE (version 3.3) was used that includes two modes, i.e. atom and pharmacophore based. The difference between the two is whether all atoms or only the pharmacophoric sites of molecules are included for analysis.<sup>30,31</sup>

For the development of 3D-QSAR models, all studied molecules were placed into a regular cubic grid (1 Å), with each cube allocated 0 or 1 “bits” to account for the different types of atomic features in training set molecules that occupy the cube. A given atom/site is deemed to occupy a cube, if the center of that cube falls within the radius of the corresponding sphere. A single cube may be occupied by more than one atom/site, and this occupation may come from the same molecule or from different molecules. Each occupied cube gives rise to one or more *volume bits*, where a separate bit is allocated for each different categories of atom/site that occupies the cubes. The total number of volume bits assigned to a given cube is based on the occupation from training set molecules. Hence, a single molecule may be represented by a string of zeros or ones, according to the cubes it occupy, and the different types of atoms/sites that reside in those cubes. For all the studied molecules, a large pool of binary values (0 to 1) is obtained, consequently these binary values are treated as independent variables for the development of QSAR model.<sup>32,33</sup>

**2.7. Partial Least Square Analysis.** PLS analysis is a combination of principal component and multiple regression analysis. It correlates dependent variables (biological activity) with independent variables (binary pool) to derive a 3D-QSAR model.

To perform PLS analysis, the “*t-value*” (eliminate variable) was set to less than 2 (<2.0) in order to improve signal-to-noise ratio and filter field descriptor with standard deviation less than 2 units obtained from PLS analysis. PHASE creates a series of regression models incorporating progressively more PLS factors with maximum number of factors being not larger than 1/5th the number of training set molecules.<sup>30,31</sup> The QSAR model was selected on the basis of highest predictive measure of the test set, i.e.  $Q^2$  (squared coefficient of correlation) and Pearson- $r$  (Pearson coefficient of correlation). The selected QSAR model should also show high values of  $R^2$  (coefficient of determination for training set molecules),  $F$ -value (Fisher test), and least value of SD (standard deviation). “ $R^2$ ” is the relative measurement of quality of internal fit of molecules. “SD” determines the variation of the predicted activity from the experimental activity and should have low value. The  $F$ -value corresponds to the variance ratio and large values indicate a more statistically significant regression.

**2.8. Validation of QSAR Model.** In order to obtain statistically significant and reliable QSAR model, it was subjected to rigorous statistical analysis. The statistical validation of the model was checked for the external prediction reliability of the model by calculating a set of other parameters e.g.  $R_o^2$  or  $R'_o^2$  close to  $R^2$  and the corresponding  $0.85 \leq k \leq 1.15$  or  $0.85 \leq k' \leq 1.15$ .<sup>34</sup>

### 3. RESULTS AND DISCUSSION

**3.1. Analysis of Active Site Water Molecules in Crystal Structures of Syk Protein.** The investigation of the active sites revealed the presence of three conserved water molecules  $W_1$ ,  $W_2$ , and  $W_3$  in three of the six crystal structures of Syk selected for protein analysis. These conserved water molecules are either participating in the binding of ligands or filling the active site. Active sites of complex 3EMG and 1XBB contain all three water molecules whereas 1XBC contains two water molecules, i.e.,  $W_1$  and  $W_2$ . The crystal structures 3FQS and 3FQH contain  $W_1$  and  $W_2$ , respectively whereas 3FQE does not contain any water molecule among the considered three water molecules. In protein complexes 3FQS, 3FQH, and 1XBC, the corresponding crystal ligand displaces the  $W_3$  from active site; thereby making it ( $W_3$ ) less significant. Thus, it was considered that only  $W_1$  and  $W_2$  may be important for determining the interactions, orientation, and position of ligands in the active site of protein during docking analysis. The stereoview of the aligned proteins with crystal ligands and important water molecules is displayed in Figure 2A and B (Supporting Information).

**3.2. Docking Analysis.** For docking analysis, 1XBB crystal structure was selected on the basis of its highest resolution of 1.56 Å. For this docking analysis, a total of four protein systems were used, i.e. 1XBB<sub>W1</sub> (1XBB with  $W_1$ ), 1XBB<sub>W2</sub> (1XBB with  $W_2$ ), 1XBB<sub>W12</sub> (1XBB with  $W_1$  and  $W_2$ ), 1XBB<sub>W0</sub> (1XBB with no water molecule). Prior performing the docking of studied molecules, the active sites of considered protein systems were validated. Six ligands were extracted out from the crystal complexes of Syk and individually docked into the active sites of the four protein systems. The best docked poses of the ligands in every protein system were checked only for their orientation and interactions. The results of this validation protocol are mentioned in Table 2. This validation protocol exhibited the high significance of protein system 1XBB<sub>W1</sub> which reproduced the experimental interactions and orientations of five (out of six) crystal ligands. The order of significance of protein systems was observed to be 1XBB<sub>W1</sub> > 1XBB<sub>W2</sub> = 1XBB<sub>W12</sub>. These three

**Table 2. Docking of Different Crystal Ligands in Protein Structure 1XBB with Different Water Molecules**

Crystal ligand	PDB ID*	Protein System 1XBB with			
		W0	W1	W2	W12
	3FQE	x	✓	✓	✓
	3EMG	✓	✓	✓	✓
	3FQH	✓	✓	✓	✓
	1XBC	x	✓	✓	✓
	1XBB	x	✓	x	x
	3FQS	x	✓	x	x
Final Score of Analysis		2/6	5/6	4/6	4/6

\*Protein Data Bank ID of corresponding crystal structure of Syk.

protein systems showed a low variation in the docking results of the six crystal ligands; thus all three were used to dock the studied molecules under consideration. The best docked pose of each ligand in terms of Glide score, essential interactions, core overlapping, proper positioning, and orientation into the active

site of protein was selected for the alignment. The best alignment of docked ligands was achieved in protein system  $1\text{XBB}_{\text{W}2}$  (i.e., with 44 out of 47 molecules) whereas the alignment of 39 and 24 molecules was obtained in protein systems  $1\text{XBB}_{\text{W}1}$  and  $1\text{XBB}_{\text{W}12}$ , respectively. During docking simulations, 39 and 24 molecules were properly accommodated into  $1\text{XBB}_{\text{W}1}$  and  $1\text{XBB}_{\text{W}12}$  while remaining failed to orient inside the active sites. Moreover, the alignment was inferior as compared to obtained with  $1\text{XBB}_{\text{W}2}$  suggesting that although in the cross docking experiments  $1\text{XBB}_{\text{W}1}$  showed better significance,  $1\text{XBB}_{\text{W}2}$  is a better choice for the docking analysis of naphthyridine analogues. Although  $\text{W}_1$  and  $\text{W}_2$  are conserved in the crystal structures, the position of  $\text{W}_1$  may not be as important of  $\text{W}_2$  and knocked out by the naphthyridine analogues in the experimental crystal-ligand complex since the chemical nature of the studied molecules is different from the studied crystal ligands and moreover the studied crystal ligands are active molecules whereas  $\text{W}_2$  is observed to be important for inactive molecules.

**3.3. Protein and Ligand Minimization.** Constrained docking is a routine analysis performed by the medicinal chemists that only considers the ligand flexibility not receptor. However, the active site flexibility of protein is sometime important to predict the more appropriate orientations and interactions of the ligands by docking analysis. A molecule, to be active or inactive, depends upon its interactions and induced conformational changes in the active site of protein. Constrained docking utilizes the same conformation of protein's active site for all range of molecules; thus the conformational changes that the ligands would induce in the active site are ignored. Therefore, in present study to consider the flexibility of active site region, the Liaison module of Schrodinger software was employed to minimize the complexes of protein and ligands obtained after Glide XP docking analysis.

The correlation between activity and free energy was observed to be  $<0.3$  in the case of tiny and small, whereas it was 0.41 in case of medium. From a total of 44 molecules, 4 were discarded as outliers, and the deletion of these molecules improved the correlation, i.e. 0.587 (Figure 3; Supporting Information). The change in conformation of the protein's active site with both active and inactive molecules is displayed in Figures 4 and 5 (Supporting Information). Finally, the ligands were extracted from selected 40 complexes and alignment was employed for development of 3D-QSAR model (Figure 6; Supporting Information).

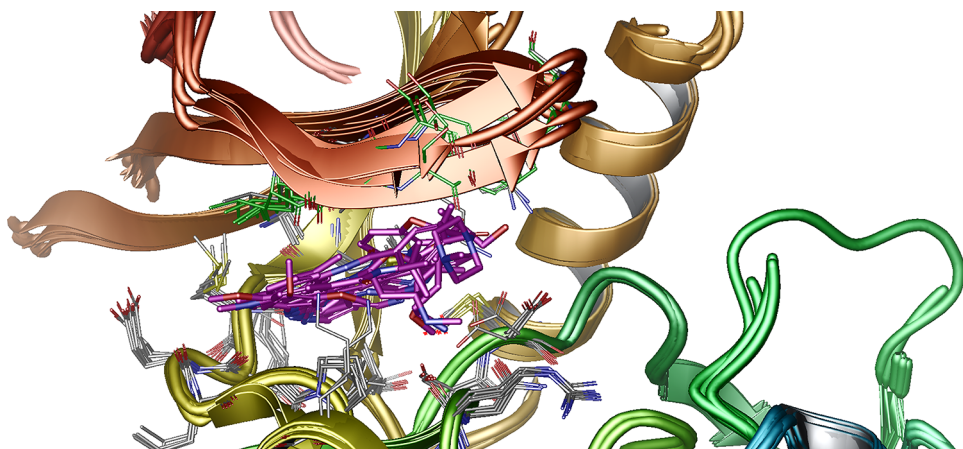


**Figure 7.** Alignment of available six protein structures.

Additionally, one more important thing was noticed after the minimization of complexes by Liaison, i.e. when the six crystal complexes were aligned, a portion of protein was observed to be highly flexible in all complexes (Figure 7). After the Liaison minimization, all 40 complexes were aligned and it was observed that the flexibility of the same part of protein was covered by Liaison minimization that supports our idea of considering the receptor flexibility using the Liaison program (Figure 8).

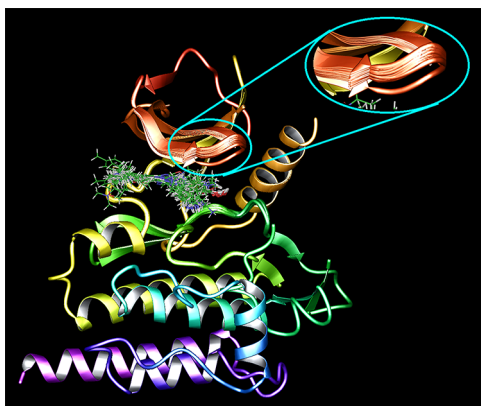


**Figure 8.** Alignment of final 40 protein–ligand complexes after the use of Liaison. In the enlarged window, the flexible region of the protein is displayed that is conserved after the use of Liaison.

**3.4. 3D-QSAR Analysis.** In order to develop the 3D-QSAR model, the data set was divided into 27 training and 13 test set molecules employing Canvas. The selected training set molecules were employed for the development of the 3D-QSAR model using five PLS factors and grid spacing of 1 Å. The QSAR model was selected corresponding to PLS factor five on the basis of the highest predictive measure for test set molecules, i.e.  $Q^2$  (0.682) and Pearson- $r$  (0.862). The selected model displayed the highest values of  $R^2$  (0.972) and  $F$ -value (146.7) and the lowest value of SD, i.e. 0.142 (Table 3). The correlation graph between the

**Table 3. Statistical Parameters<sup>g</sup> of Generated QSAR Models**

factors	SD <sup>b</sup>	R <sup>2a</sup>	F-value <sup>c</sup>	RMSE <sup>d</sup>	Q <sup>2e</sup>	Pearson- $r^f$
1	0.4086	0.751	75.2	0.50	0.586	0.778
2	0.2438	0.915	128.8	0.49	0.613	0.798
3	0.1837	0.954	157.7	0.46	0.652	0.830
4	0.1579	0.967	162.4	0.44	0.681	0.856
5	0.1332	0.978	184.5	0.44	0.682	0.862

<sup>a</sup>Correlation of prediction for training set molecules. <sup>b</sup>Standard deviation of the regression. <sup>c</sup>Variance ratio or F-test value (large values of F indicate a more statistically significant regression). <sup>d</sup>Root mean square error. <sup>e</sup>Squared coefficient of correlation for test set molecules. <sup>f</sup>Pearson coefficient of correlation for test set molecules. <sup>g</sup>Details regarding statistical parameters are given in the Supporting Information.

predicted and experimental activity of training and test set molecules on the basis of the best model is shown in Figures 9 and 10, respectively. The experimental and predicted activities of all data set molecules on the basis of the best model are mentioned in Table 4.

Additionally, a set of statistical parameters were also calculated i.e.  $k$ ,  $k'$ ,  $R_o^2$ , and  $R_o'^2$  to check the external prediction stability of the developed model. The best model showed satisfactory values

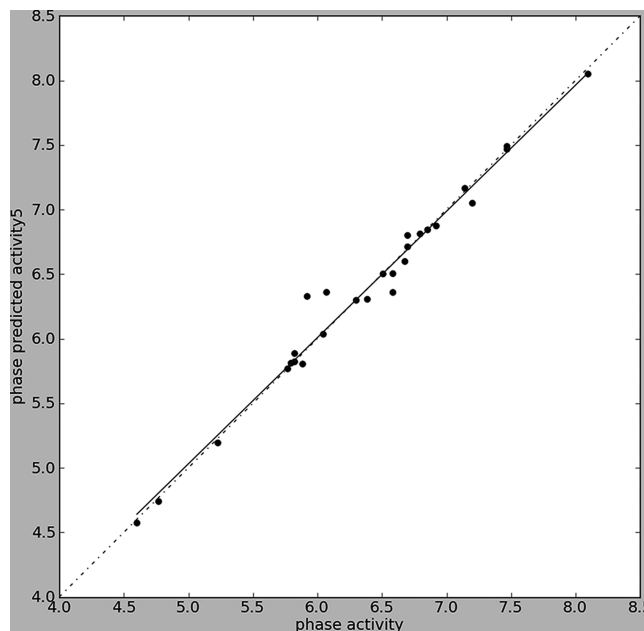


**Figure 9.** Correlation graph between experimental and predicted activities of the training set molecules.

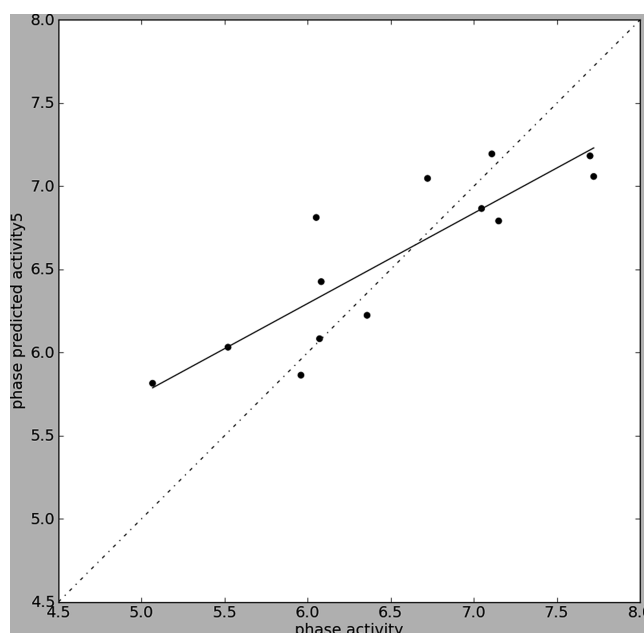


**Figure 10.** Correlation graph between experimental and predicted activities of the test set molecules.

of  $k$  0.997,  $k'$  1.000,  $R_o^2$  0.999, and  $R_o'^2$  0.999 that supported the reliability of model.

**3.5. Contour Analysis.** The contour map for hydrogen bond donor, hydrophobic, electron withdrawing property and positive ionizable group corresponding to best QSAR model is displayed in Figure 11A–D, respectively. In these figures, the most active molecule 21 (green) and the least active molecule 8 (purple) are shown as reference in the background. The blue cubes represent the favorable regions where the presence of corresponding property substituents may lead to enhancement of activity whereas vice versa for red cubes.

**3.5.1. Hydrogen Bond Donor Property Contour.** In Figure 11A, blue contour indicating region where substitution with

Table 4. Molecular Structures, Experimental, and Predicted Activities of Syk Inhibitors

Molecule ID	Structure	Biological Activity ( $\text{pIC}_{50}^{\text{a}}$ )		Molecule ID	Structure	Biological Activity ( $\text{pIC}_{50}^{\text{a}}$ )	
		Exp.	Pred.			Exp.	Pred.
1		5.824	5.821	12*		6.081	6.425
2		4.770	4.739	13		5.824	5.884
3		6.854	6.842	14*		5.520	6.031
4*		6.357	6.223	15*		5.959	5.863
5*		6.721	7.046	16		5.921	6.327
6		6.921	6.873	17		5.796	5.810
7		6.387	6.304	18		6.046	6.034
8		4.602	4.572	19		7.469	7.467
9		6.301	6.297	20*		7.699	7.182
10		6.071	6.359	21		8.097	8.049
11		6.585	6.503	22*		7.149	6.790

Table 4. continued

Molecule ID	Structure	Biological Activity ( $\text{pIC}_{50}^{\text{a}}$ )		Molecule ID	Structure	Biological Activity ( $\text{pIC}_{50}^{\text{a}}$ )	
		Exp.	Pred.			Exp.	Pred.
23		6.585	6.358	32		7.143	7.164
24		7.201	7.049	33*		7.108	7.194
25		7.469	7.489	34*		6.051	6.811
26*		7.046	6.865	35		5.770	5.766
27*		7.721	7.058	36*		5.066	5.814
28		6.678	6.597	37		6.509	6.501
29		6.699	6.799	38		5.229	5.192
30		6.796	6.811	39		5.886	5.803
31		6.699	6.711	40*		6.071	6.082

<sup>a</sup> $\text{pIC}_{50} = -\log \text{IC}_{50}$ , where  $\text{IC}_{50}$  is dose in nanomolar (nM) required to produce 50% inhibition of Syk. \*Test set molecules.

hydrogen bond donor group is favorable, is displayed at the distance of 3–4 carbons from naphthyridine ring where the presence of any hydrogen bond donor (HBD) group would enhance the potency of molecules. In the most active molecule

21, the amino group present at the terminus of the long alkyl chain (propyl) lies in the blue region (Figure 11). In other active molecules 19, 20, 22, 24, 25, 26, 32, and 33 also the terminal amino group of alkyl chain is present in the favorable blue region.

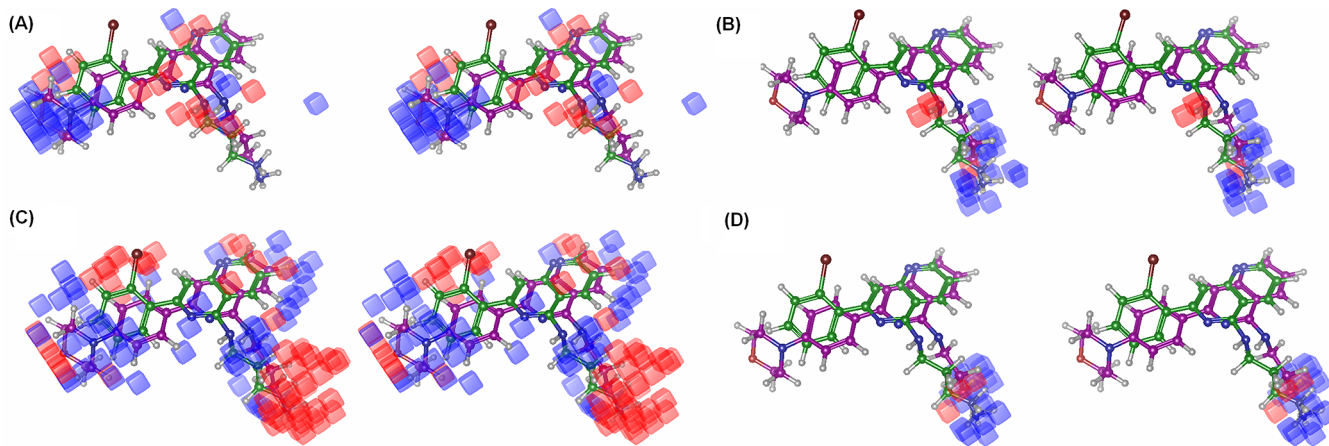


**Figure 11.** Stereoviews of contour maps for 3D-QSAR models: Hydrogen bond donor (A), hydrophobic (B), electron withdrawing property (C), and positive ionizable property (D). The highest active molecule Syk21 (green) and the least active molecule Syk8 (purple) are displayed as reference. Blue contours correspond to the regions where the substitution of corresponding property group enhances the activity and vice versa for the red contours.

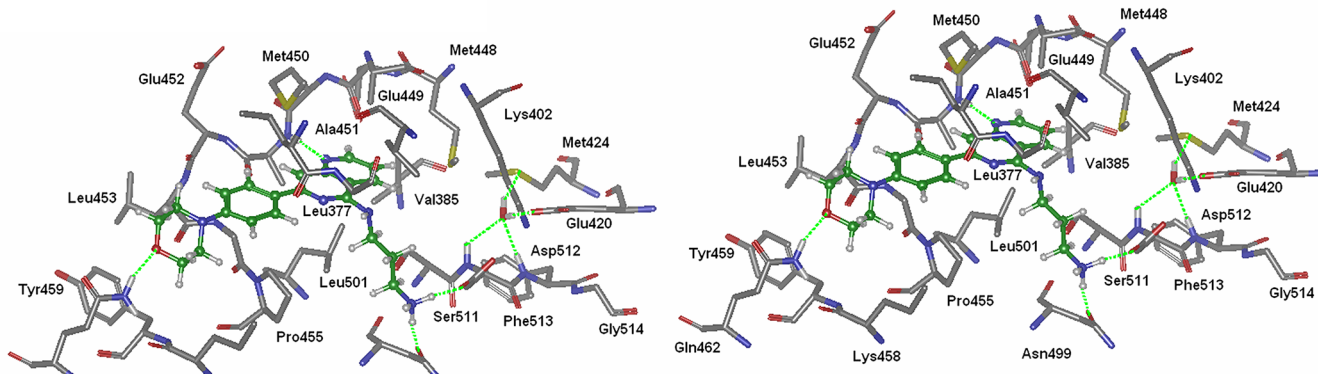


**Figure 12.** Stereoview of docking interactions of the most active molecule 21 with active site amino acid residues of protein Syk.

In the low active molecules 1, 2, 5, 8, 28, and 30, the terminal amino group is not residing in the favorable blue region due to deviation of the alkyl chain length from 3 to 4 carbons.

**3.5.2. Hydrophobic Property Contour.** A contour map for the hydrophobic property is displayed in Figure 11B. In this figure, both hydrophobic substituent favorable and unfavorable blue and red contours, respectively, are present at fifth position of naphthyridine ring which indicate that only optimal hydrophobic groups are favorable here, i.e., the groups with 3–4 carbon length (propyl group). In the highly active molecules 19, 20, 21, 24, 25, and 27 alkyl chain lies in the favorable blue region whereas low active molecule 28 with deviation in alkyl length resides its hydrophobic chain in the unfavorable red region. Substituents with bulky hydrophobic groups at this position also show detrimental effects on the activity, e.g. in low active molecules 38 (cyclohexylmethyl), 39 (3-pyridyl methyl), 35 (dimethylaminopropyl), and 40 (3-methylaminobenzyl), bulky hydrophobic groups lie in the unfavorable red region.

The presence of favorable blue contours at the meta and para position of the benzene ring present at the seventh position of the naphthyridine ring indicate that in molecules 19, 20, 21, 24, 25, and 27 a favorable hydrophobic group is present at this position. On the other hand, an unfavorable red contour is present at the ortho position of the same benzene ring that indicates the unsuitability of ortho position for hydrophobic substituents. The least active molecule 8 bears a bromine group at this position that may be responsible for the steric clashes with the active site

amino acid residues, i.e., Met 450 and Leu 377 of protein. Moreover, the blue contours present at the third position of the naphthyridine ring confer this position favorable for the substituent of hydrophobic groups, e.g. molecule 6 bearing a bromine group at this position is more active than unsubstituted molecule 3.

**3.5.4. Positive Ionizable Contour.** The positive ionizable property contour map is displayed in Figure 11D. In this figure, positive ionizable substituent favorable blue contours are present at a distance of 3–4 carbons from the naphthyridine nucleus. The presence of suitable positive ionizable groups in these contours would favor the activity of molecules. For instance in highly active molecules 19, 20, 21, and 27, positively ionized groups ( $-NH_3^+$ ) are present at the terminal of alkyl chain resides in blue regions. In other low active molecules 1, 2, 5, 27, 28, and 30, the positively ionizable group ( $-NH_2$ ) is not residing in the favorable blue region.

**3.5.5. Electron Withdrawing Contour.** In Figure 11C, the contour map for the electron withdrawing property is displayed. A blue colored favorable region is present at the para position of the benzene ring which indicates that the electron withdrawing atoms (O and N) at this position are favorable. In the most active molecule 21, two electron withdrawing atoms N and O (as per PHASE manual) are present in the blue regions. In the case of other highly active molecules 19, 20, 23, 25, and 27, the electron withdrawing atom N is present in these contours. On the other hand, low active molecules 13, 17, and 18 are devoid of such

electron withdrawing atoms at the para position, thereby showing low activity.

The presence of both hydrophobic and electron withdrawing substituent favorable blue contours at the para position of the benzene ring clearly indicates that position is suitable for the hydrophobic groups attached to high electron density atoms (O, N).

**3.6. Validation of Contours Using Docking Analysis.** To check the reliability of generated contours, the results of docking analysis were used for comparison. Figure 12 displays the conformation of the most active molecule 21 in the active site of protein Syk after the use of Glide XP and Liaison. In the figure, a molecule is bound to the active site of the protein by forming a network of H-bonding and hydrophobic interactions. Hydrogen bonds are displayed as four interactions i.e. terminal amino ( $-\text{NH}_2$ ) group of ligand with Asp512 ( $\text{N}\cdots\text{O}$ ; 2.52 Å) and Asn499 ( $\text{N}\cdots\text{O}$ ; 2.63 Å) amino acid residues of protein. Other H-bonds are between the N atom of napthyridine ring (1st position) with Ala451 ( $\text{N}\cdots\text{N}$ ; 3.02 Å) and the oxygen of morpholine ring with Gln462 ( $\text{O}\cdots\text{N}$ ; 2.90). In addition to these H-bonding interactions, a molecule is fitted in the active site by forming strong hydrophobic interactions with Tyr459, Lys454, Leu501, Pro455, Gly378, Val385, and Leu377 amino acid residues.

The HBD contours present at the terminus of alkyl chain are well complemented with H-bonding interactions of the terminal amino group with Asp512 and Asn499. The hydrophobic interactions of the ligand molecule with Lue453, Pro455, Tyr459, Val385, Leu377, and Leu501 amino acid residues also validate the positions of hydrophobic contours.

**3.7. Validation of the Present Analysis with Reported Pharmacophore Analysis.** Xie et al. have reported a three-dimensional pharmacophore analysis of a large number of diverse Syk inhibitors.<sup>35</sup> The pharmacophore model consisted of four structural features, i.e. one hydrogen bond donor, hydrogen bond acceptor, ring aromatic, and hydrophobic feature each. In the report, the authors proposed the docking interactions and the mapping of pharmacophore model over staurosporin which describes that the hydrogen bond acceptor (HBA) feature corresponds to carbonyl "O" of the pyrrole-2-one motif, HBD to the methyl amine in the tail of staurosporine, the ring aromatic (RA) feature to the central pyrrole, and the hydrophobic (HY) feature to the benzene ring fused with the pyrrole ring. The docking interactions of staurosporine molecules are displayed as two H-bonding interactions, i.e. an HBA feature with Ala451 and HBD feature with Arg498. The hydrophobic feature is surrounded by Leu377, Gly454, and Pro455. The generated model was employed as a 3D query for retrieving potential inhibitors from different chemical databases such as NCI, MayBridge, Specs, and CNPD.

In the present study, 3D-QSAR analysis was performed using a set of 1,6-napthyridine Syk inhibitors. 3D-QSAR analysis is different from pharmacophore modeling in its applicability. Pharmacophore modeling is a method of lead identification whereas 3D-QSAR is a method of lead optimization. Although, the two approaches are different, the models generated for them share common features. Both models suggested that the hydrophobic substituent is favorable at the seventh, hydrogen bond acceptor at the fifth, and hydrogen bond donor at the first positions of the 1,6-napthyridine nucleus. In addition to this, the present 3D-QSAR analysis also revealed other structural requirements (as discussed in the Contour Analysis section) of

the molecules that would help to design new and potent congeneric molecules.

**3.8. Role of Water Molecules.** The structural water molecule  $W_2$  was explored in the docking analysis for determining the orientation and conformation of studied molecules within the active site of Syk. The analysis clearly revealed that  $W_2$  makes H-bonds with active site amino acids and fills the space of active site and this filling determines the orientation and conformation of the molecules. Furthermore, the importance of  $W_2$  was also determined by docking coupled with Liaison minimization for the molecules reported in literature in the presence of  $W_2$  and comparing with docking results in the absence of  $W_2$  (i.e. with  $W_1$  alone and without any water molecule).

The docking analysis of napthyridine derivatives showed that the docking energy of the low active molecules show good correlation with the biological activity in the  $1\text{XBB}_{W_2}$  protein system as compared with the  $1\text{XBB}_{W_0}$  protein system. In the low active molecules, the bulky substituents present at the fifth position of 2-oxyindole ring shows the changes in the conformations due to steric clashes with the water molecule which tend to increase the docking energy and develop a good correlation with biological activity of molecules. In the absence of this water molecule, the bulky substituents fill the cavity and show remarkably lower docking energy i.e. similar to the docking energy of highly active molecules and display poor correlation with biological activity of molecules. This water is highly conserved by forming strong interactions with protein and is not displaced out by the bulky substituents so the clashes of the bulky groups with this water would be the reason for their low activity. Similarly, the docking analysis of imidazo[1,2c]pyrimidine, pyrimidine-5-carboxamide, and 1,2,4-triazolo[4,3c]pyrimidine derivatives also display a similar pattern as shown by napthyridine derivatives. Thus, the conserved water molecule would especially help to determine the better poses of the low active molecules which will be in good correlation with the activity.

**3.9. Designing of New Syk Inhibitors.** The information revealed from the generated contour plots was utilized to design new molecules. The interpretation of contours helped to locate the sites of napthyridines for substitution with different groups that can improve the activity. The optimal features for napthyridines were interpreted as (1) the fifth position of napthyridines should have an alkyl chain of 3–4 carbons with positively ionized ( $-\text{NH}_3^+$ ) and hydrogen bond donor ( $-\text{NH}_2$ ,  $-\text{CONH}_2$ ,  $-\text{OH}$ ) groups at the terminal of this chain and (2) the seventh position should have a hydrophobic group attached through a electron withdrawing atom (O, N, and S; Figure 13). Accordingly, 80 new molecules were designed and same procedure was employed for their processing and activity prediction. Molecular structures and predicted activities of the top 11 molecules are mentioned in Table 5.

**3.10. Absorption, Distribution, Metabolism, and Excretion (ADME) Property Calculations of Newly Designed Molecules.** Newly designed Syk inhibitors were analyzed for ADME properties using the QikProp program of Maestro 9.2. Determination of ADME properties is an essential guide for the lead generation that can avoid the failure of drug candidates in later stages due to poor pharmacokinetic profile. The drug likeness of the newly designed Syk inhibitors was analyzed by Lipinski's rule of five and other pharmacokinetic parameters required for absorption, distribution, metabolism, and excretion (Table 6). Lipinski's rule states that any drug

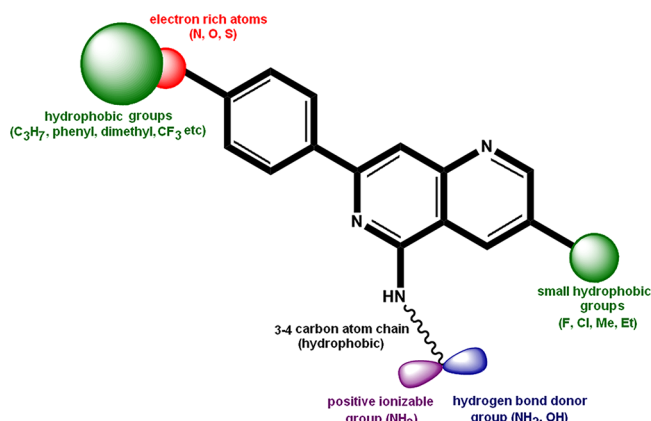


**Figure 13.** Preferable substituent sites of naphthyridine nucleus for the designing of new candidates.

should comply with following criteria to become orally active (a) " $<5$  hydrogen bond donors", (b) " $<10$  hydrogen bond acceptors", (c) " $<500$  Da molecular mass", (d) " $<5$  an octanol–water partition coefficient ( $\log P$ )". All newly designed molecules comply with Lipinski's rule of five, thus are drug-like. Other ADME parameters like partition coefficient ( $Q\text{PlogPo/w}$ ) and water solubility ( $Q\text{PlogS}$ ), required for the evaluation of absorption and distribution of drugs within the body, ranged between 2.6 and 4.7 and  $-4.1$  and  $-5.8$ , respectively. Cell permeability ( $Q\text{PPCaco}$ ), critical for drug metabolism and excretion, ranged from 43.7 to 320.1. The calculated/estimated percental human oral absorption ranged from 72 to 100 for all molecules. All the calculated parameters are within the acceptable range, thus the designed 11 molecules can be considered as orally active for human use.

**Table 5. Molecular Structures and Predicted Activity Values of Newly Designed Syk Inhibitors**

Molecule	Structure	Predicted activity ( $\text{pIC}_{50}$ )	Molecule	Structure	Predicted activity ( $\text{pIC}_{50}$ )
Des 1		6.518	Des 6		6.850
Des 2		6.539	Des 7		7.016
Des 3		6.590	Des 8		6.535
Des 4		6.666	Des 9		6.713
Des 5		6.716	Des 10		6.560
			Des 11		6.709

**Table 6.** ADME Properties of 11 Newly Designed Syk Inhibitor Molecules Using the Qikprop Module of Maestro 9.2

designed molecules	mol. wt	QPlogPo/w <sup>a</sup>	QPlogS <sup>b</sup>	QPlogHERG <sup>c</sup>	QPPCaco <sup>d</sup>	QPPMDCK <sup>e</sup>	percent human oral absorption <sup>f</sup>
Des1	353.4	3.7	-4.3	-6.6	284.8	255.3	92.4
Des2	410.8	4.7	-5.3	-6.7	320.1	1807.0	100.0
Des3	403.6	4.7	-5.8	-6.8	246.7	120.5	100.0
Des4	426.6	3.2	-4.5	-6.8	60.1	26.2	77.6
Des5	393.5	4.3	-5.3	-6.7	265.6	236.8	95.6
Des6	394.4	4.3	-4.6	-6.5	308.7	1239.1	96.7
Des7	416.5	2.8	-4.1	-6.8	60.0	47.4	75.1
Des8	355.9	3.5	-4.4	-6.6	215.0	256.8	89.0
Des9	395.9	4.1	-5.4	-6.6	196.4	232.7	92.0
Des10	349.5	3.7	-4.2	-6.4	260.9	128.1	91.6
Des11	418.9	2.6	-4.3	-6.8	43.7	46.0	71.6

<sup>a</sup>Predicted octanol/water partition coefficient log P (acceptable range: -2.0–6.5). <sup>b</sup>Predicted aqueous solubility: S in moles per liter (acceptable range: -6.5–0.5). <sup>c</sup>Predicted IC<sub>50</sub> value for blockage of HERG K<sup>+</sup> channels (concern below -5.0). <sup>d</sup>Predicted Caco-2 cell permeability in nanometers per second (acceptable range: <25 is poor and >500 is great). <sup>e</sup>Predicted apparent MDCK cell permeability in nanometers per second. <sup>f</sup>Percentage of human oral absorption (<25% is poor and >80% is high).

## 4. CONCLUSION

In the present study, we constructed a statistically reliable 3D-QSAR model using inhibitory activity of 47 naphthyridine derivatives against Syk enzyme. For this purpose docking based alignment was utilized considering importance of two structural water molecules as well as active site flexibility of protein through Liaison program of Maestro 9.2. On the basis of generated 3D-QSAR model, new Syk inhibitors were designed and their activities were predicted. These newly designed Syk inhibitors can be synthesized in a rational and cost-effective manner and can also be explored as novel therapeutic agents in the treatment of inflammatory disease conditions including multiple sclerosis, rheumatoid arthritis, and bronchial asthma.

## ASSOCIATED CONTENT

### Supporting Information

Figures 2–6, structures of the four molecules removed as outliers in Liaison minimization, and Details regarding statistical parameters of the QSAR model. This material is available free of charge via the Internet at <http://pubs.acs.org>.

## AUTHOR INFORMATION

### Corresponding Author

\*E-mail: omsilakari@rediffmail.com. Tel.: +919501542696.

### Notes

The authors declare no competing financial interest.

## ACKNOWLEDGMENTS

The authors thank Dr. Ravikumar Muttineni (Application Scientist), Er. Anirban Banerjee (IT Consultant), and Mr. Raghu Rangaswamy from Schrödinger, Bangalore, for their constant scientific and technical support to handle Schrödinger software and work smoothly. The authors also thank University Grant Commission, New Delhi, for providing the financial support; Grant No. 37-324/2009(SR).

## REFERENCES

- (1) Pamuk, O. N.; Tsokos, G. C. Spleen tyrosine kinase inhibition in the treatment of autoimmune, allergic and autoinflammatory diseases. *Arthritis Res Ther.* **2010**, *12*, 222.
- (2) <http://www.rcsb.org/pdb>.
- (3) Pivniouk, V. I.; Martin, T. R.; Lu-Kuo, J. M.; Katz, H. R.; Oettgen, H. C.; Geha, R. S. SLP-76 deficiency impairs signaling via the high affinity IgE receptor in mast cells. *J. Clin. Invest.* **1999**, *103*, 1737.
- (4) Pine, P. R.; Chang, B.; Schoettler, N.; Banquerigo, M. L.; Wang, L.; Lau, A.; Zhao, F.; Grossbard, E. B.; Payan, D. G.; Brahn, E. Inflammation and bone erosion are suppressed in models of rheumatoid arthritis following treatment with a novel Syk inhibitor. *Clin. Immunol.* **2007**, *124*, 244.
- (5) Kurosaki, T.; Takata, M.; Yamanashi, Y.; Inazu, T.; Taniguchi, T.; Yamamoto, T.; Yamamura, H. Syk activation by the Src family tyrosine kinase in the B cell receptor signaling. *J. Exp. Med.* **1994**, *179*, 1725.
- (6) Meltzer, E. O.; Berkowitz, R. B.; Grossbard, E. B. An intranasal Syk-kinase inhibitor (R112) improves the symptoms of seasonal allergic rhinitis in a park environment. *J. Allergy Clin. Immunol.* **2005**, *115*, 791.
- (7) Cywin, C. L.; Zhao, B. P.; McNeil, D. W.; Hrapchak, M.; Prokopowicz, A. S., III; Goldberg, D. R.; Morwick, T. M.; Gao, A.; Jakes, S.; Kashem, M.; Magolda, R. L.; Soll, R. M.; Player, M. R.; Bobko, M. A.; Rinker, J.; DesJarlais, R. L.; Michael, P.; Wintersb, M. P. Discovery and SAR of Novel [1,6]naphthyridines as potent inhibitors of spleen tyrosine kinase (SYK). *Bioorg. Med. Chem. Lett.* **2003**, *13*, 1415–1418.
- (8) Hirabayashi, A.; Mukaiyama, H.; Kobayashi, H.; Shiohara, H.; Nakayama, S.; Ozawa, M.; Miyazawa, K.; Misawa, K.; Ohnata, H.; Isaji, M. A novel Syk family kinase inhibitor: Design, synthesis, and structure activity relationship of 1,2,4-triazolo[4,3-c]pyrimidine and 1,2,4-triazolo[1,5-c]pyrimidine derivatives. *Bioorg. Med. Chem.* **2008**, *16*, 7347–7357.
- (9) Hirabayashi, A.; Mukaiyama, H.; Kobayashi, H.; Shiohara, H.; Nakayama, S.; Ozawa, M.; Tsuji, E.; Miyazawa, K.; Misawa, K.; Ohnata, H.; Isaji, M. Structure activity relationship studies of imidazo[1,2-c]pyrimidine derivatives as potent and orally effective Syk family kinases inhibitors. *Bioorg. Med. Chem. Lett.* **2008**, *16*, 9247–9260.
- (10) Hisamichi, H.; Naito, R.; Toyoshima, A.; Kawano, N.; Ichikawa, A.; Orita, A.; Orita, M.; Hamada, N.; Takeuchi, M.; Ohtaa, M.; Tsukamoto, S. Synthetic studies on novel Syk inhibitors. Part 1: Synthesis and structure activity relationships of pyrimidine-5-carboxamide derivatives. *Bioorg. Med. Chem.* **2005**, *13*, 4936–4951.
- (11) Farmer, L. J.; Bemis, G.; Britt, S. D.; Cochran, J.; Connors, M.; Harrington, E. M.; Hoock, T.; Markland, W.; Nanthakumar, S.; Taslimi, P.; Haar, E. T.; Wang, J.; Zhaveri, D.; Salituro, F. G. Discovery and SAR of novel 4-thiazolyl-2-phenylaminopyrimidines as potent inhibitors of spleen tyrosine kinase (SYK). *Bioorg. Med. Chem. Lett.* **2008**, *18*, 6231–6235.
- (12) Bajpai, M. Fostamatinib, a Syk inhibitor prodrug for the treatment of inflammatory diseases. *IDrugs* **2009**, *12*, 174–185.
- (13) Singh, R.; Masuda, E.; Bhamidipati, S.; Sun, T.; Stella, V. J. *Prodrugs of 2,4-pyrimidinediamine compounds and their uses*. Rigel Pharmaceuticals Inc. Patent Number WO2006/078846.
- (14) Yu, J.; Clough, J.; Singh, R. *2,4-Pyrimidinediamine compounds and their uses*. Rigel Pharmaceuticals Inc. Patent number WO0306379.
- (15) Singh, R.; Argade, A.; Li, H.; Bhamidipati, S.; Carroll, D.; Sylvain, C.; Clough, J.; Keim, H. *Rigel Pharmaceuticals Inc. Methods of treating or*

- preventing autoimmune diseases with 2,4-pyrimidinediamine compounds. Rigel Pharmaceuticals Inc. Patent number WO2004/014382.
- (16) Clough, J.; Bhamidipati, S.; Singh, R.; Masuda, E.; Haoran, Z. 2,4-Pyrimidinediamine compounds for use in the treatment or prevention of autoimmune diseases. Rigel Pharmaceuticals Inc. Patent number WO2005/012294.
- (17) Cooper, R.; Singh, R.; Clough, R. Spiro-2,4-pyrimidinediamine compounds and their uses. Rigel Pharmaceuticals Inc. Patent number WO2006/068770.
- (18) Taylor, S. C. J. Xinafoate salt of n4-(2, 2-difluoro-4hbenz[1,4]Oxazin-3-one)-6-yl]-5-fluoro-N2-[3-(methylaminocarbonylmethyleneoxy)phenyl]2,4-pyrimidinediamine. Pfizer Limited. Patent number WO2009/031011
- (19) Kashem, M. A.; Nelson, R. M.; Yingling, J. D.; Pullen, S. S.; Prokopowicz, A. S., III; Jones, J. W.; Wolak, J. P.; Rogers, G. R.; Morelock, M. M.; Smow, R. J.; Homon, C. A.; Jakes, S. Three mechanistically distinct kinase assays compared: measurement of intrinsic ATPase activity identified the most comprehensive set of ITK inhibitors. *J. Biomol. Screen.* **2007**, *12*, 70–83.
- (20) Maestro, version 9.2; Schrödinger, LLC, New York, 2011.
- (21) Ligprep, version 2.5; Schrödinger, LLC, New York, 2011.
- (22) Glide, version 5.6; Schrödinger, LLC, New York, NY, 2010.
- (23) Friesner, R. A.; Banks, J.; Murphy, R. B.; Halgren, T. A.; Klicic, J.; Mainz, D. T.; Repasky, M. P.; Knoll, E. H.; Shaw, D. E.; Shelley, M.; Perry, J. K.; Francis, P.; Shenkin, P. S. Glide: a new approach for rapid, accurate docking and scoring. 1. Method and assessment of docking accuracy. *J. Med. Chem.* **2004**, *47*, 1739–1749.
- (24) Atwell, S.; Adams, J. M.; Badger, J.; Buchanan, M. D.; Feil, I. K.; Froning, K. J.; Gao, X.; Hendle, J.; Keegan, K.; Leon, B. C.; Muller-Deickmann, H. J.; Nienaber, V. L.; Noland, B. W.; Post, K.; Rajashankar, K. R.; Ramos, A.; Russell, M.; Burley, S. K.; Buchanan, S. G. A novel mode of Gleevec binding is revealed by the structure of spleen tyrosine kinase. *J. Biol. Chem.* **2004**, *279*, 55827–55832.
- (25) Farmer, L. J.; Bemis, G.; Britt, S. D.; Cochran, J.; Connors, M.; Harrington, E. M.; Hoock, T.; Markland, W.; Nanthakumar, S.; Taslimi, P.; Haar, E. T.; Wang, J.; Zhaveri, D.; Salituro, F. G. Discovery and SAR of novel 4-thiazolyl-2-phenylaminopyrimidines as potent inhibitors of spleen tyrosine kinase (SYK). *Bioorg. Med. Chem. Lett.* **2008**, *18*, 6231–6235.
- (26) Villasenor, A. G.; Kondru, R.; Ho, H.; Wang, S.; Papp, E.; Shaw, D.; Barnett, J. W.; Browner, M. F.; Kuglstatter, A. Structural insights for design of potent spleen tyrosine kinase inhibitors from crystallographic analysis of three inhibitor complexes. *Chem. Biol. Drug Des.* **2009**, *73*, 466–470.
- (27) Liaison, version 5.7; Schrödinger, LLC, New York, NY, 2011; Strike, version 2.0; Schrödinger, LLC, New York, NY, 2011.
- (28) Canvas, version 1.4, Schrödinger, LLC, New York, NY, 2011.
- (29) Duan, J.; Dixon, S. L.; Lowrie, J. F.; Sherman, W. Analysis and comparison of 2D fingerprints: Insights into database screening performance using eight fingerprint methods. *J. Mol. Graph. Model* **2010**, *29*, 157–170.
- (30) PHASE, version 3.3; Schrödinger, LLC, New York, NY, 2011.
- (31) Dixon, S. L.; Smolyrev, A. M.; Knoll, E. H.; Rao, S. N.; Shaw, D. E.; Friesner, R. A. PHASE: A new engine for pharmacophore perception, 3D-QSAR model development and 3D database screening. 1. Methodology and preliminary results. *J. Comput. Aided Mol. Des.* **2006**, *20*, 647–671.
- (32) Evans, D. A.; Doman, T. N.; Thorner, D. A.; Bodkin, M. J. 3D-QSAR Methods: Phase and Catalyst Compared. *J. Chem. Inf. Model* **2007**, *47*, 1248–1257.
- (33) Mehta, N.; Chand, S.; Bahia, M. S.; Silakari, O. Elaboration of New Anti-Inflammatory Agents Using Pharmacophore Based 3D-QSAR of 4, 5-Diaryl Imidazoline as P2 × 7 Receptor Antagonists. *Lett. Drug Des. Discov.* **2012**, *9*, 185–198.
- (34) Golbraikh, A.; Tropsha, A. Beware of q2! *J. Mol. Graph. Model* **2002**, *20*, 269–276.
- (35) Xie, H.; Li, L.; Ren, J.; Zou, J.; Yang, L.; Wei, Y.; Yang, S. Pharmacophore modeling study based on known Spleen tyrosine kinase inhibitors together with virtual screening for identifying novel inhibitors. *Bioorg. Med. Chem. Lett.* **2009**, *19*, 1944–1949.